Bending Flexibility of Actin Filaments during Motor-Induced Sliding

Petr G. Vikhorev, Natalia N. Vikhoreva, and Alf Månsson
School of Pure and Applied Natural Sciences, University of Kalmar, Kalmar, Sweden

ABSTRACT Muscle contraction and other forms of cell motility occur as a result of cyclic interactions between myosin molecules and actin filaments. Force generation is generally attributed to ATP-driven structural changes in myosin, whereas a passive role is ascribed to actin. However, some results challenge this view, predicting structural changes in actin during motor activity, e.g., when the actin filaments slide on a myosin-coated surface in vitro. Here, we analyzed statistical properties of the sliding filament paths, allowing us to detect changes of this type. It is interesting to note that evidence for substantial structural changes that led to increased bending flexibility of the filaments was found in phalloidin-stabilized, but not in phalloidin-free, actin filaments. The results are in accordance with the idea that a high-flexibility structural state of actin is a prerequisite for force production, but not the idea that a low-to-high flexibility transition of the actin filament should be an important component of the force-generating step per se. Finally, our data challenge the general view that phalloidin-stabilized filaments behave as native actin filaments in their interaction with myosin. This has important implications, since phalloidin stabilization is a routine procedure in most studies of actomyosin function.

INTRODUCTION

Muscle contraction is the result of cyclic interactions between globular units of myosin II and actin molecules in the thin filaments of the sarcomere (1,2). A widely accepted view of the molecular events is that force and motility are produced by ATP-induced structural changes in the myosin head and neck domains, with the actin filaments acting mainly as passive binding and force-transmitting partners (2). However, the actin filaments are highly dynamic, and several studies have provided evidence that binding of various regulatory proteins (3–6) or myosin motor domains (7–17) is associated with significant structural changes, most likely cooperatively propagated (4,13,15,18,19) along the filaments. Some of these structural changes lead to reduced flexural rigidity of the actin filaments (7,12,16,17). These results, taken together with other findings (5,9,20), have formed the basis for theories (e.g., (17,21,22)) that the actin filaments are more active players in muscle contraction than is generally believed (2,23,24).

If ATP is added to actin filaments in solution simultaneously with myosin motor fragments, the effects on the filaments are more complex than in the absence of ATP. These effects include induction of faster and larger bending motions (25), or evidence for an increase in the effective temperature for tangential motion of the filaments (26). These effects have been attributed either to dynamic structural changes in the actin filaments per se (17) or to hydrodynamic forces generated by the swing of the myosin lever arm (26).

The above-cited results were obtained with actomyosin in solution. However, if structural changes in the actin filaments, e.g., those reflected in altered flexural rigidity, are really important for actomyosin motor function, they should also be present when the filaments are propelled by myosin motors. This situation (as in the in vitro motility assay) differs from that with actomyosin in solution in several important respects. In addition to the active transportation of the actin filaments relative to the motors, there are rather few myosin heads attached to actin at each given time, and these exist in a distribution of different structural and chemical states. Moreover, the myosin heads are strained to various degrees (also placing local strain on the actin filament) due to their fixed immobilization sites on the surface. Naturally, the latter fact also presents an obstacle that so far has prevented studies of actin filament flexural rigidity under myosin-induced translation.

It is interesting to note that theoretical arguments (27) have been put forth that it should be possible to derive the persistence length (proportional to the flexural rigidity) from the statistical properties of the paths of heavy-meromyosin (HMM)-propelled actin filaments. The persistence length of kinesin-propelled microtubule paths (28–30) was measured in recent studies. However, due to a length-dependent persistence length in this case (31), it is not straightforward to relate the observed path persistence lengths to the persistence length of microtubules (32). Whereas no length dependence of the persistence length is expected for actin filaments (33,34), there may be other uncertainties in equating the path persistence length with the filament persistence length. First, myosin heads that bind to the filament (away from the filament axis) are known to apply a torque (35) that may add an unspecified component to reduce the path persistence length. Second, there could be complex hydrodynamic effects of

Submitted June 23, 2008, and accepted for publication September 2, 2008.

Address reprint requests to Alf Månsson, School of Pure and Applied Natural Sciences, University of Kalmar, SE-391 82 Kalmar, Sweden. Tel.: 46-480-446243; Fax: 46-480-446262; E-mail: alf.mansson@hik.se.

Editor: Yale E. Goldman.

0006-3495/08/12/5809/11 $2.00

doi: 10.1529/biophysj.108.140335

myosin binding in the presence of ATP, as described for filaments in solution (17,26). Finally, the path persistence length may be affected by ordering effects (36) that could occur with a high density of motors adsorbed to a surface, as in most motility assay experiments. Thus, whereas the model of Duke et al. (27) seems reasonable for an ideal system, there is no firm evidence that it correctly reproduces the behavior in real experiments. This uncertainty is emphasized by very recent results (37) that give a persistence length of 8.8 μm for the paths of HMM-propelled actin filaments (see also (9) for related results). This value is considerably lower than the persistence length of 15–18 μm reported by several authors (3,6,17,32,38,39) for phalloidin-stabilized filaments in solution (in the absence of myosin).

In contrast to the above inconclusive and partly conflicting results, we here present evidence to corroborate the idea (27) that the path persistence length directly reflects the persistence length of the motor-propelled filaments. On the basis of these results, we then provide evidence for a large change in the persistence length as a result of actomyosin motor activity. However, this effect was only observed with phalloidin-stabilized actin filaments, the routine preparation in most functional studies of actin-myosin interactions.

The results are discussed in relation to the mechanisms of contractile activation and actomyosin motor function. Moreover, the often-held view (e.g., (14,15)) that phalloidin-stabilized filaments behave like native actin filaments in their interaction with actin is challenged.

THEORY

The changes in sliding direction due to thermal motion of the leading end of myosin-propelled actin filaments may be presumed to result in curved filament paths (27) characterized by the path persistence length, L_P, as defined below. (L_P denotes the persistence length of the actin filament path (P). The quantities L_A^S and L_A^L refer to persistence lengths of the actin filaments (A) rather than the path. The superscript ''S'' indicates that the measurements were made with the actin filaments freely suspended in solution, and the superscript ''L'' indicates that the measurement is of the free leading end of an HMM-propelled actin filament.) In this connection, it is relevant to study the autocorrelation of the path velocity vector ($\overline{v}(t)$) with the velocity vector at the onset of measurements ($\overline{v}(0)$; i.e., the initial velocity vector). The following relationship applies for the derivative of the autocorrelation function:

$$\frac{d}{dt}\langle \overline{v}(t)\cdot\overline{v}(0)\rangle = \frac{d}{ds}\langle \overline{v}(s)\cdot\overline{v}(0)\rangle\frac{ds}{dt} = v_f^3\frac{d}{ds}\langle \overline{u}(s)\cdot\overline{u}(0)\rangle, \tag{1}$$

where s is the distance along the filament path ($ds/dt \equiv v_f$; sliding speed) and $\overline{u}(s)$ and $\overline{u}(0)$ are unit tangent vectors at path lengths s and 0, respectively. Now, we can proceed as in Howard (40) (pp. 317–318), showing that

$$\begin{aligned}\frac{d}{dt}\langle \overline{v}(t)\cdot\overline{v}(0)\rangle &= v_f^3\frac{d}{ds}\langle \overline{u}(s)\cdot\overline{u}(0)\rangle \\ &\approx -v_f^3\left\langle\frac{1}{2}\left(\frac{\Delta\theta}{\Delta s}\right)^2\Delta s\right\rangle\langle \overline{u}(s)\cdot\overline{u}(0)\rangle \\ &= -v_f^3\frac{\langle E_{elastic}\rangle}{EI}\langle \overline{u}(s)\cdot\overline{u}(0)\rangle \\ &= -v_f^3\frac{kT}{2EI}\langle \overline{u}(s)\cdot\overline{u}(0)\rangle \\ &= -(v_f^3/2L_A^L)\langle \overline{u}(s)\cdot\overline{u}(0)\rangle. \end{aligned}\tag{2}$$

Here, $\Delta\theta$ is the random angular change in sliding direction (for a sliding distance Δs related to the length of the freely fluctuating leading end of the actin filament) and $\langle E_{elastic}\rangle$ is the average elastic energy of this free end. Moreover, $L_A^L = EI/kT$ is its persistence length. The product kT is the Boltzmann factor, whereas EI is the flexural rigidity of the actin filament. The relationship $\langle E_{elastic}\rangle = kT/2$ is derived from equipartition of energy, assuming that the free end of the actin filament executes thermal fluctuations in a plane.

The solution of the differential equation (Eq. 2) gives

$$\langle \overline{u}(t)\cdot\overline{u}(0)\rangle = \langle\cos(\theta(s)-(\theta(0))\rangle = \exp(-v_f t/(2L_A^L)), \tag{3}$$

and if we define the persistence length of the filament path in an analogous way to the filament persistence length (i.e., for the two-dimensional case (41)),

$$\langle \overline{u}(t)\cdot u(0)\rangle = \exp(-v_f\, t/(2L_P)), \tag{4}$$

it is clear that $L_P = L_A^L$. Since L_A^L is determined by the actin filament structure and material properties, it is clear that L_P is not affected by the average length of the free fluctuating end of the filament as long as there is more than one myosin head attached (27), and that some further preconditions are met. Thus, it is important that there is no buckling of the leading end of the filament, and the relaxation time for the thermal oscillations of the leading end must be sufficiently fast (27). As illustrated by the calculations below, these conditions are likely to apply in the experiments described here.

At sliding velocities and motor densities similar to those in this work, there is evidence that the free leading end of the filament has an average length, L, of <0.10 μm (42). The time (t_p) it takes for the filament to be propelled the distance L (μm) would be L s μm^{-1} (<0.10 s) and 0.1 L s μm^{-1} (<0.01 s) at sliding velocities of 1 and 10 μm s^{-1}, respectively. The relaxation time, τ, for thermal fluctuations of the free leading end of the filament, assuming that it is clamped at the first myosin head, is given by the expression (40)

$$\tau < \frac{c_\perp L^4}{EI(\pi/2)^4}. \tag{5}$$

Here, $c_\perp$ is the drag coefficient/unit length (5.5×10^{-15} Ns μm^{-2}, based on a surface-to-filament distance of 15 nm) (43) for translation of the actin filament in a direction perpendic-

ular to its long axis. The quantity EI (here, 7×10^{-14} N μm^2) (32) is the flexural rigidity of the filament.

The condition ensuring sufficient time for equilibration of the thermal fluctuations of the free leading end of the filament is that $\tau/t_p \ll 1$. That this condition is fulfilled is clear from the following calculations: insertion of numerical values into Eq. 5 gives $\tau < \sim 0.013$ s μm$^{-4} L^4$, i.e., $\tau/t_p < 0.13$ μm$^{-3} L^3$ (see above) for the present conditions ($v_f < 10$ μm s^{-1}) or, explicitly, $\tau/t_p < 1.3\ 10^{-4} \ll 1$, as $L < 0.10$ μm.

Buckling due to viscous forces occurs if (27,40)

$$L > \sim \left(\frac{EI}{v_f c_\parallel} \right)^{1/3}, \quad (6)$$

where $c_\parallel$ is the drag coefficient/unit length (2×10^{-15} Ns μm^{-2} based on a surface-to-filament distance of 15 nm) (40) for translation of the actin filament in a direction parallel with its long axis. By inserting numerical values of EI and $c_\parallel$, and setting $v_f = 10$ μm s^{-1}, it is clear that buckling occurs only if $L > \sim 1.5$ μm, i.e., it does not occur in practice.

MATERIALS AND METHODS

Surface preparations, protein preparations, and in vitro motility assays

Myosin was purified from rabbit back muscle and HMM was produced by digestion of myosin using TLCK-treated α-chymotrypsin (44). The HMM was frozen in the presence of 2 mg ml^{-1} sucrose in liquid nitrogen and stored at –80°C until use. Actin was extracted from rabbit skeletal muscle acetone powder (45). Polymerization of G-actin in G-buffer (2 mM Tris-HCl, pH 8.0, 0.2 mM Na_2ATP, 0.2 mM $CaCl_2$, 0.5 mM dithiothreitol, and 1 mM NaN_3) was initiated by adding 1 mM $MgCl_2$ and 50 mM KCl. Actin filaments were fluorescently labeled with *N*-hydroxysuccinimide (NHS)-rhodamine with expected labeling of Lys-113 (46). The labeling was performed using the EZ-Label Rhodamine Protein Labeling Kit (Pierce, Rockford, IL) according to the manufacturer's protocol. The labeling stoichiometry was determined based on a procedure recommended by the supplier of the dye conjugate and it was found to be 0.4 mol dye/mol actin. Aliquots of labeled and unlabeled F-actin were frozen in liquid nitrogen and stored at −80°C for up to 7 months. Before use, samples were thawed and either used without phalloidin stabilization or labeled overnight with regular nonfluorescent phalloidin or Alexa-488 phalloidin (Molecular Probes, Invitrogen, Eugene, OR) at a 1:2 (actin/phalloidin) ratio. Both preparations of fluorescently labeled actin were stored on ice for up to 1–2 days before use. Protein concentrations were measured using the Bradford assay (Sigma-Aldrich, St. Louis, MO). The purity and integrity of actin with and without NHS-rhodamine were analyzed by 12% sodium dodecyl sulfate polyacrylamide gel electrophoresis (Fig. 1).

The observation solution (buffer A) contained 10 mM MOPS (3-(*N*-morpholino) propanesulfonic acid, pH 7.4), 1 mM $MgCl_2$, 0.1 mM EGTA, 10 mM dithiothreitol, an oxygen-scavenging system (3 mg ml^{-1} glucose, 0.1 mg ml^{-1} glucose oxidase, and 0.02 mg ml^{-1} catalase), and appropriate amounts of KCl, to produce ionic strengths of 40, 80, or 130 mM. In some motility assay experiments 0.6% methylcellulose (MC) was added. The buffers are designated A40, A80, and A130 (buffer A without MC; ionic strength 40, 80, or 130 mM) and A80MC and A130MC (buffer A with MC; ionic strength 80 or 130 mM).

In vitro motility assay experiments were performed using trimethylchlorosilane-functionalized coverslips (47). ATP-insensitive HMM was removed by pelleting at 336,000 *g* for 30 min in the presence of F-actin and ATP (44). Flow cells were incubated with HMM (120 μg ml^{-1}, 2 min), bovine serum albumin (BSA; 1 mg ml^{-1}, 30 s), fluorescently labeled actin (10–20 nM, 30 s), and, finally, assay buffer of appropriate ionic strength (Buffer A) with MgATP (1 mM), creatine phosphate (2.5 mM), and creatine kinase (56 units ml^{-1}). In some experiments, HMM incubation concentrations of either 60 or 30 μg ml^{-1} were used. The temperature was maintained either at 23 ± 1.2 (range) or at 29 ± 0.7°C. At each experimental occasion, temperature was constant within ±0.5°C.

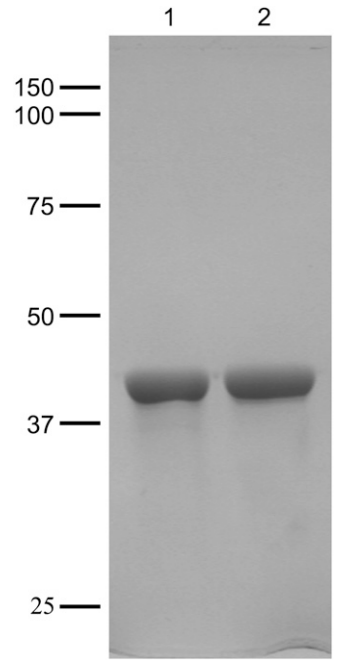

FIGURE 1 Sodium dodecyl sulfate polyacrylamide gel electrophoresis of actin preparation used in the experiments described in this study. Both lanes represent preparation after freezing and thawing: *lane 1*, actin without NHS-rhodamine; *lane 2*, actin labeled with NHS-rhodamine. Note the high degree of purity and, in particular, the complete absence of any bands corresponding to tropomyosin and troponin components. Numbers to the left of the gel refer to the molecular mass (in kDa).

Actin filaments were visualized with a Nikon Eclipse TE 300 inverted microscope equipped with 100×, NA 1.4 oil immersion objective (Nikon, Tokyo, Japan) under epifluorescence illumination. Image sequences were recorded using a cooled Hamamatsu EMCCD-camera (C9100-12; Hamamatsu, Hamamatsu City, Japan). The sequences were analyzed with respect to actin filament sliding velocity and the fraction of motile filaments using software (48,49) developed in the Matlab enviroment (The MathWorks, Natick, MA).

Analysis of the persistence length of actin filament paths

The persistence length of a two-dimensional filament path may be defined on the basis of the velocity autocorrelation function (see above) or the related quantity, $\langle \cos\theta(s) - \theta(0)) \rangle$, the cosine correlation function.

Experimentally, $\theta(s)$ and s were obtained by tracking actin filaments in the in vitro motility assay. This was achieved using a Matlab program (see below; Supplementary Material, Data S1) applied to image sequences recorded using the EMCCD-camera. The pixel magnification in the images was 0.16×0.16 μm^2 pixel^{-1} and the frame rate was 3–10 s^{-1} (chosen on the basis of the actin sliding velocity). In the analysis process, the leading end of the filament was tracked interactively using the computer pointer device. Filaments a distance of 20 μm or more from the image edge were selected for tracking.

The numerical value of L_P was obtained by fitting a single-exponential function (Eq. 3) to the data: $y(s) = \cos(\theta(s) - \theta(0))$ for all filaments and all

relevant values of the path length, s. To facilitate viewing of the data before fitting, they were pooled in groups containing s-values distributed within a range of 1 μm. The average value of all data points representing $\cos(\theta(s) - \theta(0))$ in this range was then located in a position given by the average s-value. Next, nonlinear regression was performed, taking into account the variability in the $\cos(\theta(s) - \theta(0))$ data and the total number of data points. The fitting was limited to path lengths <20 μm, but since tracking was performed for longer path lengths than this, several independent paths could be obtained from one sliding filament.

During tracking and analysis, special care was taken to eliminate abrupt and large changes in sliding direction, e.g., caused by defect myosin heads (50) that may lead to local buckling of the actin filament. Even if such events are rare, they may introduce significant errors in the analysis due to potentially large magnitudes. However, effects of this type may be minimized by excluding paths with angular changes in sliding direction between frames of $>\sim$4 standard deviations of the narrow Gaussian peak fitted to the distribution of such changes (see the Supplementary Material, Data S1). In practice, if an abrupt change in sliding direction, according to the above definition, was detected before the filament had been tracked in four subsequent frames, the entire path was excluded from the analysis. Otherwise, the path was used for analysis up to the image frame immediately before the onset of the abrupt change. The described procedure would ensure that all relevant filament paths were included, whereas those exhibiting large changes in sliding direction, e.g., due to the presence of rigor heads, would be excluded, thereby minimizing effects on the determination of persistence length.

Experimental procedure for determination of actin filament flexibility in solution

A flow cell was constructed from one small coverslip placed on a glass slide using melanine-resin-based rhodamine-B-marked microparticles of 1 μm diameter (Sigma-Aldrich, St. Louis, MO) as spacers (38). This produced a flow cell of 2–4 μm in height as determined by grading of the objective focusing knob. Before the assembly of the flow cell, surfaces were soaked in BSA (1 mg ml^{-1}) and dried. The actin filaments (10–20 nM) in buffers A40, A80, or A130 with an oxygen scavenger system were infused in a flow cell by capillary forces. In some experiments, MgATP (1 mM), creatine phosphate (2.5 mM), and creatine kinase (56 units ml^{-1}) were also added to the buffer. The flow cell was sealed with vacuum grease (Dow Corning, Midland, MI) and allowed to set for 1–2 h. The time interval was limited to 1 h in the case of NHS-rhodamine-labeled actin filaments in buffer A40 (due to a tendency for depolymerization). Filaments executing two-dimensional Brownian motion were observed by fluorescence microscopy and recorded using the Hamamatsu EMCCD-camera (exposure time $<$0.03 s; pixel magnification 0.32 $\times$ 0.32 μm^2 pixel^{-1}). The resulting images were then used for measurements to allow calculation of the persistence length, L_A^S, of actin filaments in solution, using Eq. 3. In this version the variable s is taken as the contour length of the filament from one end and L_A^L is exchanged for L_A^S. The contour lengths used for the fits were <10 μm due to limited length of the filaments. One given filament was examined only once to avoid correlation effects in the experimental data. The experiments were performed at a temperature of 23 $\pm$ 1.2°C.

Statistical analysis

Curve fittings and statistical analyses were performed using the GraphPad Prism software (version 5.00; GraphPad Software, San Diego, CA).

RESULTS

Typical examples of sliding paths of HMM-propelled actin filaments in the in vitro motility assay are illustrated for phalloidin-free (Ph$^-$; NHS-rhodamine-labeled) and phalloidin-stabilized (Ph$^+$) filaments in Fig. 2. Moreover, the insets of this figure show examples of images of actin filaments in solutions, which were used to derive the actin filament persistence length (L_A^S). The path persistence length was obtained by tracking the leading end of the filaments. However, the path traced out by this end was generally very similar to that of the rest of the filament, with only minor fluctuations (9). This may be inferred from the generally narrow paths in Fig. 2. These paths are reconstructed by overlaying images of entire filaments in $\sim$50 subsequent frames in an image sequence and therefore represent all parts of a sliding filament. The observation that all parts of a filament seem to trace out a similar path is consistent with the view that all the parts are propelled by the same population of myosin heads. This is in accordance with the view that the sliding direction is determined by thermal fluctuation of the free leading end of the filaments (29).

The persistence length, L_A^S, of actin filaments freely suspended in solution in the absence of HMM was measured under different experimental conditions. The results in Fig. 3 *A* for phalloidin-stabilized (Ph$^+$; *shaded*) and phalloidin-free (Ph$^-$; *solid*) filaments are in accordance with previous results (3,6) showing that L_A^S was significantly higher for Ph$^+$ than for Ph$^-$ filaments. Moreover, the results suggest a nearly rectilinear increase of L_A^S with increased ionic strength. The slope in linear regression analysis was 0.046 $\pm$ 0.0014 μm mM^{-1} for Ph$^-$ filaments (different from 0; $p \approx 0.02$) and 0.045 $\pm$ 0.007 μm mM^{-1} for Ph$^+$ filaments (n.s.; $p \approx 0.10$). Experiments at an ionic strength of 80 mM (A80 solution; Fig. 3, *B* and *C*) suggested that L_A^S for Ph$^+$ filaments was similar whether phalloidin stabilization was achieved using

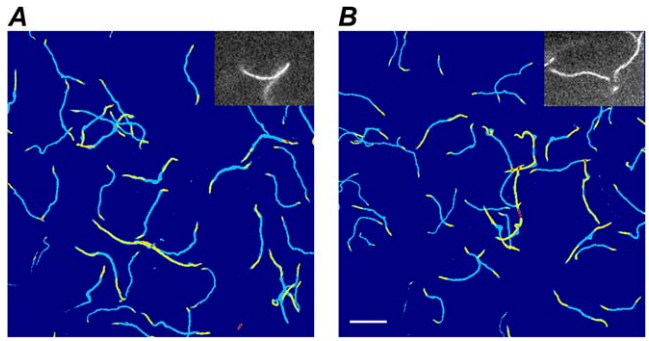

FIGURE 2 Filament paths and free fluctuating filaments in A80 solution at 23°C. (*A*) Paths (*light blue*) of HMM-propelled actin filaments without phalloidin (Ph$^-$) obtained by overlaying 50 subsequent epifluorescence microscopy images. Images acquired at a frame rate of 10 s^{-1} over a total of 5 s. The filament position at the onset of recording and after 4.8 s is indicated by yellow markers. Red parts of paths correspond to overlap of the leading end of the filament at the onset of recording with the trailing end of the filament after 4.8 s, which occurred for very long filaments. In addition, some positions where filament paths cross are color-coded in red. (*Inset*) Example of a grayscale image of Ph$^-$ filaments (labeled with NHS-rhodamine) in solution, used for determination of L_A^S. (*B*) The same type of image as in *A*, but for Ph$^+$ filaments (labeled with Alexa-488 phalloidin). Scale bar, 10 μm.

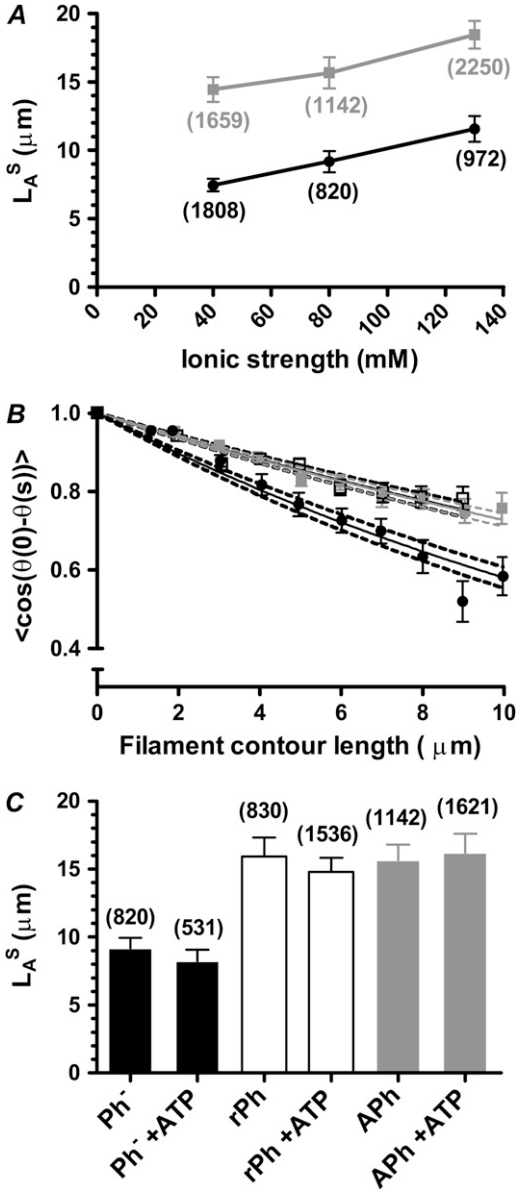

FIGURE 3 Persistence lengths (L_A^S) of actin filaments in solution. (*A*) Actin filaments with (*shaded squares*) or without (*solid circles*) phalloidin. Ph^+ filaments were stabilized with APh and Ph^- filaments were fluorescence-labeled with NHS-rhodamine. The temperature was 23 ± 1.2°C, and there was no MgATP in the observation solution. The numerical value of L_A^S was obtained by fitting Eq. 3 to experimental data (total number of data points in parentheses) from two to four flow cells and 82–238 filaments for each experimental condition. (*B*) Cosine correlation functions for actin filaments in solution (A80). Individual data points (from 57–179 filaments) are given with error bars (mean ± SE). Data for Ph^- filaments (*solid circles*) and for Ph^+ filaments labeled with APh (*shaded*) or with rPh + NHS-rhodamine (*open squares*). Equation 3 was fitted to the data (*solid lines*) by nonlinear regression and shown with 95% confidence bands (*dashed lines*). (*C*) Numerical values of L_A^S for Ph^- filaments (*solid*) in the absence (four flow cells) and presence (three flow cells) of MgATP. Data are also given for Ph^+ filaments labeled with 1), rPh (*open bars*) in the absence (three flow cells) and presence (four flow cells) of MgATP; and 2), APh (*shaded*) in the absence and presence of MgATP (three flow cells for each case). The number of data points used for fitting of Eq. 3 is given in parentheses. Error bars in panels *A* and *C* represent 95% confidence intervals for L_A^S obtained in the nonlinear regression analysis.

fluorophore-free regular phalloidin (rPh) or Alexa-488 phalloidin (APh). Moreover, the difference in L_A^S between Ph^+ and Ph^- filaments was similar whether MgATP (and creatine kinase/creatine phosphate) was present or not (Fig. 3 *C*).

Both Ph^+ (cf. (51).) and Ph^- actin filaments were fully functional in the in vitro motility assay, with >75% motile filaments in both cases but consistently higher sliding velocities for the Ph^- than for the Ph^+ filaments (Fig. 4 *A*) (cf. (52).). The effects of Ph stabilization on sliding velocity was particularly noticeable at low ionic strength, and occurred for filaments that were labeled with both APh and rPh (Fig. 4 *B*).

The path persistence length (L_P) increased with increased ionic strength of the assay solution (Fig. 5, *A* and *B*) at two

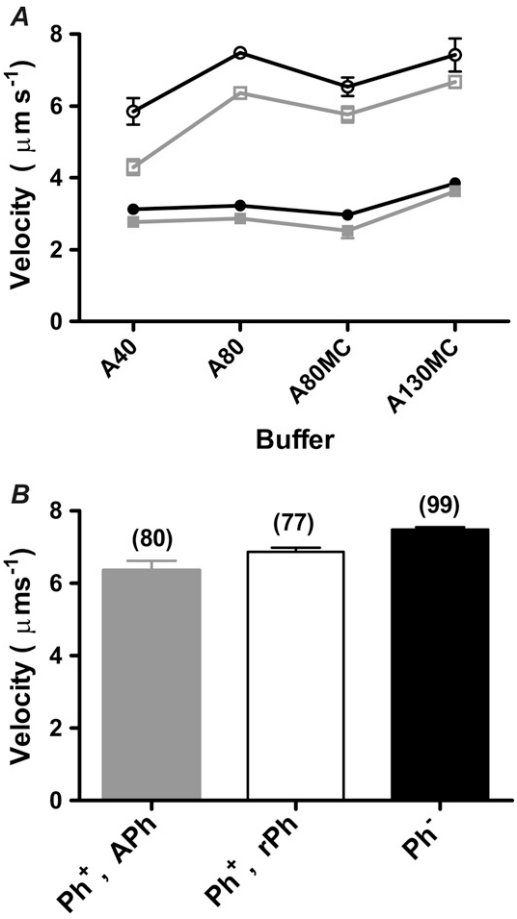

FIGURE 4 Sliding velocity of HMM-propelled actin filaments labeled with Alexa-488 phalloidin (*shaded squares*) or NHS-rhodamine (*solid circles*). Error bars represent 95% confidence intervals. (*A*) Experiments were performed in solutions of different ionic strength (40–130 mM) in the absence (*A40*, *A80*) and presence of methylcellulose (*A80MC*, *A130MC*), at 23 ± 1.2°C (*solid symbols*) or 29 ± 0.7°C (*open symbols*). Data for each condition were obtained from 17–138 filament paths using three to six flow cells, except in the cases of A40 data at high temperature (one flow cell) and MC data at low temperature (two to three flow cells). Error bars represent 95% confidence intervals. (*B*) Velocity data obtained in A80 solution (2–4 flow cells), comparing the effects of phalloidin stabilization with APh and rPh. Numbers in parentheses represent the number of filament paths analyzed.

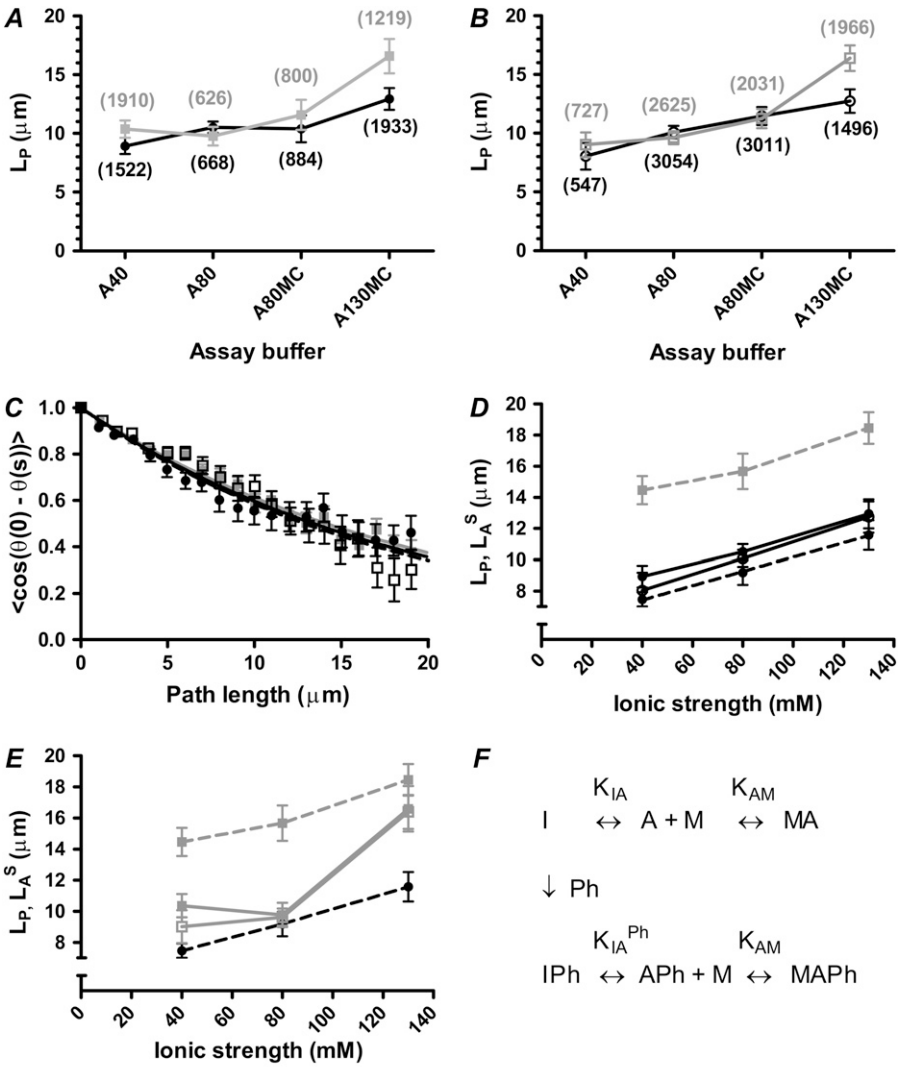

FIGURE 5 Persistence lengths of actin filament paths. Ph^+ and Ph^- filaments are represented by shaded squares and solid circles, respectively. (*A*) L_P data at 23 ± 1.2°C. (*B*) L_P data at 29 ± 0.7°C. Data in *A* and *B* were derived by fitting of Eq. 3 to the cosine correlation function. Error bars represent 95% confidence intervals. Numbers in parentheses indicate the total number of data points from 27–155 filaments (each tracked for one or two independent trajectories of 20 μm length) for each fit (condition). Experiments were the same as in Fig. 4. (*C*) Cosine correlation functions for HMM-propelled filament paths in A80 solution for Ph^- (*solid circles*) and Ph^+ filaments (*shaded squares*, APh; *open squares*, rPh). Lines represent fits of Eq. 4 to the data by nonlinear regression. Plotted average data (mean ± SE) are based on a total of 1400–3240 individual data points. (*D*) L_P data for the Ph^- filaments in *A* and *B* (*shaded symbols* and *shaded lines*; A80MC data omitted) superimposed on L_A^S data (*dashed lines*; from Fig. 3 *A*) for both Ph^+ (*shaded*) and Ph^- (*solid*) filaments. (*E*) L_P data for the Ph^+ filaments in *A* and *B* (*shaded symbols* and *shaded lines*) superimposed on L_A^S data (*dashed lines*; from Fig. 3 *A*) for both Ph^+ (*shaded*) and Ph^- (*solid*) filaments. (*F*) Kinetic scheme, developed from Kozuka et al. (14), representing different actin filament structural states in inactive (*I* and *IPh*) and active (*A*, *APh*, *MA*, and *MAPh*) conformations. The binding of phalloidin is assumed to be irreversible on the experimental timescale. Otherwise, equilibria are assumed to exhibit rapid kinetics (14) (equilibrium constants K_{IA}, K_{IA}^{Ph}, and K_{AM}). For details, see text.

different temperatures (23 and 29°C). At these temperatures there was a twofold difference in sliding velocity, with small expected differences (12) in filament persistence length. For Ph^- filaments, the slope of the persistence length versus ionic strength (linear regression) was 0.045 ± 0.003 μm mM^{-1} (different from 0; $p \approx 0.046$) at 23°C and 0.052 ± 0.008 μm mM^{-1} (n.s.; $p \approx 0.10$) at 29°C. It is of interest to note that these slopes are quantitatively very similar to those seen for the plot of L_A^S versus ionic strength (Fig. 3). In the calculation of the regression lines, the average values of the A80 and A80MC data were used for the data point at 80 mM ionic strength. For Ph^+ filaments, L_P was increased with ionic strength from 80 to 130 mM, but no significant difference was seen between the values at 40 and 80 mM.

Of interest, and in contrast to L_A^S, the value of L_P was not affected by the presence of phalloidin, except at 130 mM ionic strength. Thus, for ionic strengths of both 40 and 80 mM, the 95% confidence intervals for the L_P values of Ph^+ and Ph^- filaments overlapped at both 23 and 29°C. The lack of any phalloidin effect on L_P was confirmed in A80 solution both for APh and rPh filaments (Fig. 5 *C*). Moreover, results obtained at an ionic strength of 80 mM suggested that the presence of methylcellulose in the assay solution did not appreciably affect the measured value of L_P (Fig. 5, *A* and *B*).

By combining the data in Fig. 4 and Fig. 5, *A* and *B*, it is clear that there is no correlation between the numerical values of L_P and the filament sliding velocity ($r = 0.134$; not significantly different from zero).

In Fig. 5, *D* and *E*, the L_A^S data from Fig. 3 have been replotted (*dashed lines*) and superimposed on L_P values from Fig. 5, *A* and *B*. Fig. 5 *D* shows that the numerical values of L_P and L_A^S for Ph^- filaments were not significantly different at any ionic strength tested (overlap of 95% confidence intervals). Accordingly (see above), the plots of L_P and L_A^S against ionic strength exhibited virtually identical slopes. In contrast, Fig. 5 *E* shows that L_P for Ph^+ filaments was significantly different from L_A^S of such filaments at 40 and 80 mM ionic strengths. Instead, under these conditions, L_P for the Ph^+ filaments was similar to L_A^S for the Ph^- filaments. However, at an ionic strength of 130 mM, the L_P and L_A^S values for the Ph^+

filaments were quite similar, although the L_P value in this case was also slightly lower than that for L_A^S.

We also performed experiments with low-HMM incubation concentrations (30 and 60 μg ml^{-1} instead of 120 μg ml^{-1}) causing the average sliding velocity to be reduced to $<$50% of that at saturating HMM densities. These experiments were based on filament paths from only one flow cell for each condition. However, they were not repeated since they gave results that were very similar either to earlier results (52) or to the data above. Thus, as in the previous experiments with different degrees of phalloidin labeling (52), the lower sliding velocity of Ph$^+$ compared to Ph$^-$ filaments at high HMM incubation concentrations could not be reproduced at the lowest incubation concentration tested. Second, as with the data at higher HMM incubation concentrations, there was no significant difference between L_P data for Ph$^+$ and Ph$^-$ filaments when using HMM incubation concentrations of 30 or 60 μg ml^{-1}.

DISCUSSION

Methodological considerations

The motility assay procedure and the data analysis algorithms were optimized to achieve conditions allowing comparison of L_P and the persistence length of filaments in solution (L_A^S) under the idealized conditions of the theoretical model described above. This means that the progressive changes in sliding direction should only be governed by thermal fluctuations of the leading filament end. Abrupt changes in sliding direction, such as those caused by the presence of ATP-insensitive heads (see further discussion in the Supplementary Material, Data S1), should be eliminated. This also applies to collective ordering effects and other effects (e.g., nanoscale topographical features (53)) that tend to bias the sliding direction.

The removal of filament paths with abrupt direction changes was achieved by the analysis algorithm described in some detail in Materials and Methods (see also the Supplementary Material, Data S1). The use of very smooth surfaces in the form of silane monolayers (47) ensured that no new topographical features were introduced by the surface derivatization. Finally, omission of blocking actin, normally employed to block ATP-insensitive heads, was important to minimize tendencies for ordering effects.

The complications that may be introduced by the presence of blocking actin deserve further comments. Under normal motility assay conditions (incubation with 1 μM of blocking actin), the density of blocking actin filaments (nonfluorescent) can be quite substantial during the actual motility assay experiment (54). This can have (at least) two effects that may cause disturbances in the cosine correlation function. First, high filament and motor densities predispose to collective ordering effects (36). This has the potential to cause apparently increased persistence length of the filament paths and, in contrast to what we observed experimentally, a substantial deviation of the experimental data from the single-exponential equation (Eqs. 3 and 4). Second, there is the risk (quite substantial (P. G. Vikhorev, N. N. Vikhoreva. and A. Mansson, unpublished)) that nonfluorescent filaments in the background anneal to the leading end of fluorescent filaments (without being detected). According to the model (see above), this would be expected to cause the statistical properties of the filament path to be influenced by the properties of blocking actin. These properties may differ from those of the fluorescent filaments under study.

Here, we solved the problems related to blocking actin simply by eliminating it from the assay. By the use of actin affinity centrifugation to remove rigorlike heads, this was possible with maintained high sliding velocities (see below) and a high fraction of motile actin filaments.

The use of actin filaments without phalloidin stabilization was central in this study. We found that such filaments could be observed for $>$1 h after dilution to a concentration below critical for polymerization. Although there was an increased tendency for depolymerization, particularly at low ionic strength (A40 solution), the actin filaments were quite stable. In motility assays, the possibility exists that myosin binding stabilized the polymerized state of actin (55), and accordingly, motility assays at a very low degree of phalloidin labeling have also been performed by others (52). However, filaments in solution have also previously been observed for appreciable time periods (56,57).

Persistence length in solution: relation to previous results

The persistence length of actin filaments in solution has mainly been studied using phalloidin-labeled filaments. One of the most detailed studies, testing a range of polymerization conditions, was that of Isambert et al. (3). This study gave values for Ph$^+$ filaments (polymerized with physiological salts) in the range 15.5–17 μm, similar to the values in this study, 14.5–18.5 μm. These findings are also consistent with results from several other studies (6,17,32,38,39), giving persistence length values in the range 15–18 μm. All the cited results were based on measurements with actin filaments freely suspended in solution. In contrast, a lower persistence length (8.75 μm) of Ph$^+$ filaments was obtained by fitting a wormlike chain model to the length-tension relation of actin filaments stretched between microfabricated cantilevers (58). The reason for the low value in the latter study is not immediately clear. The possibility exists that tension in the filaments (58) or the attachment to the cantilevers via the actin-binding protein α-actinin could affect the results. Whether α-actinin affects the actin filament persistence length is unknown, but other actin binding proteins have been shown to have such effects (6). Moreover, it is also known that binding of a protein at one actin filament end may induce structural changes that propagate for long distances along the filament (4,13,15,18,19).

There are a limited number of studies of persistence length of Ph$^-$ filaments in solution. However, Isambert et al. (3) and

Greenberg et al. (6) found persistence length values in the range 8.5–11 μm, in good agreement with the data in this study, in the range 7.5–11.6 μm.

There are also numerous investigations of the actin filament persistence length after deposition of the filaments on surfaces (13,16,59,60), mainly using electron microscopy. However, these methods may give rise to ambiguities in different respects (3,41), making detailed quantitative comparisons to the above-cited data (3,6,17,32,38,39) difficult.

To summarize, most available data seem to suggest that Ph^+ filaments in solution have a persistence length in the range of 15–18 μm (slightly variable at different ionic strengths). Similarly, Ph^- filaments seem to exhibit persistence lengths in the range 8–11 μm. However, it is also clear from the literature (58) that some uncertainty remains about the absolute values. Moreover, there have been indications (60) that subtle differences in polymerization conditions may produce actin filaments with varying flexibility. For these reasons, a critical element of this study was the measurement of both L_A^S and L_P with actin filaments polymerized under the same well-defined conditions.

Persistence length of actin filaments during motor activity

Changes in bending flexibility of actin filaments has been associated with certain specific changes in actin filament structure (16,34). According to the theoretical reasoning above (see also Duke et al. (27)), such changes in bending flexibility of sliding actin filaments should be reflected in the persistence length of the filament paths (L_P).

If the actin filament bending flexibility is unaffected by actomyosin motor activity, the persistence length of the filaments in solution, and of the free leading end of a sliding filament, would be equal, i.e., $L_A^S = L_A^L$. Therefore, since L_A^L cannot be measured directly in any obvious way, the idea (27) that $L_A^L = L_P$ may instead be tested experimentally by comparing the numerical values of L_P and L_A^S under different experimental conditions.

Our results showed that the numerical values of L_P and L_A^S, for Ph^- filaments, were not significantly different at any given ionic strength. This finding is consistent with the views that 1), the bending flexibility of Ph^- actin filaments does not change to any appreciable degree during actomyosin motor activity; and 2), $L_P = L_A^L$, in accordance with theory. That the striking similarities between L_P and L_A^S at different ionic strengths and temperatures (representing a range of sliding velocities) should instead be the fortuitous result of a combination of various complicating factors seems highly unlikely. As discussed above, we also took precautions to eliminate certain experimental complications. Issues such as a length-dependent persistence length, which have previously complicated studies of kinesin-propelled microtubules (29,30), are not a problem with actin filaments (34). Moreover, in a very recent study (37) of L_P for HMM-propelled actin filaments, no direct comparisons were made with the persistence length of filaments in solution. Therefore, the results presented here may be regarded as the strongest available experimental evidence for the validity of the theoretical relationship $L_P = L_A^L$.

The numerical value of L_P for Ph^+ filaments was similar to L_A^S for Ph^- filaments at the two lowest ionic strengths tested. This can be explained 1), if $L_P = L_A^L$ also for the Ph^+ filaments, and 2), if actomyosin motor activity causes a switch of Ph^+ filaments into a high-flexibility conformation (16) similar to that for Ph^- filaments. The existence of only two such discrete flexibility states has been proposed previously (16), and is consistent with the clustering of L_P and L_A^S data (for a given ionic strength) around either a well-defined low or high value (see above in Discussion).

Substantial changes in L_A^L upon motor activity, as suggested by the L_P data for Ph^+ filaments (Fig. 5 *E*), imply structural changes in the sliding actin filament that have propagated several monomers toward the leading (minus) end (27) of the filament. If the small difference between L_P and L_A^S for Ph^+ filaments at 130 mM ionic strength is viewed in this context, the possibility emerges that it is attributed to a failure of propagation of local myosin-induced structural changes in actin, rather than to the lack of such changes. That the smaller difference between L_P and L_A^S for Ph^+ filaments at 130 mM ionic strength should instead be due to the presence of methylcellulose in the assay solution is unlikely, since methylcellulose did not have such effects at 80 mM ionic strength (Fig. 5, *A* and *B*).

Yanagida and Oosawa (7) presented evidence for reduced bending flexibility of phalloidin-free actin filaments in ghost fibers upon binding of HMM in the absence of ATP. This suggests that either the larger number of bound myosin heads per filament length or the absence of motor activity may lead to different effects on filament flexibility than in this study. Alternatively, there may be poor propagation along the filament of local myosin-induced structural changes for the Ph^- filaments in this work (cf. 130 mM ionic strength for Ph^+ filaments). However, the fact remains that L_P attains very similar values for Ph^+ and Ph^- filaments at low ionic strengths. The most straightforward interpretation of this observation is that both Ph^+ and Ph^- filaments are in the same high-flexibility state during HMM-propelled sliding. In accordance with this view, the L_P values (at least at 40 and 80 mM ionic strength) were similar to the lowest L_A^S values observed in solution (3,6).

Persistence lengths and changes in actin filament structure during actomyosin interactions

Phalloidin stabilization of the actin filament structure seems to involve structural changes in subdomain 2 of the actin monomer (60,61). Moreover, structural changes in this region, particularly of the DNase I binding loop, have been

associated with the switch between high and low flexibility states (16,33). Accordingly, it has been suggested (16) that changes in subdomain 2 are the basis for increased flexibility of the actin filament upon myosin binding in the absence of ATP. The importance of subdomain 2 or the subdomain 2/subdomain 1 interface, for actomyosin interaction and force generation, accords with evidence from spectroscopy (14) and cross-linking (62) experiments (see also (11)).

A recent fluorescence resonance energy transfer (FRET) study (14) was performed with the donor probe attached to Gln-41 (in the DNase I binding loop) and the acceptor probe to Cys-374 in subdomain 1. This study, with labeled monomers sparsely incorporated into the actin filament, suggested that motor activity was associated with a shift of the equilibrium between different actin filament structural states, from a myosin-inactivating low-FRET state (*I*) to a myosin-activating high-FRET state (*A*). If effects of phalloidin (*Ph*) and myosin (*M*) are included, this idea may be represented by the kinetic scheme in Fig. 5 *F*. This scheme accounts for the FRET data (14) (obtained in the presence of phalloidin) if $K_{IA}^{Ph} \approx 1$, since equal time was spent by the filament in the I and A states in the absence of motor activity. Upon motor activity, the active states were stabilized (14), corresponding to a high value of K_{AM} in the scheme in Fig. 5 *F*.

It seems reasonable that the low- and high-flexibility states, observed here, are related to the I and A states, respectively, of Kozuka et al. (14). We thus propose that the high-flexibility state of the filament corresponds to complete domination of the high-FRET A state. This idea would accommodate both our data describing a low-to-high flexibility switch of Ph^+ filaments upon motor activity and previous data (14) showing a complete shift toward the A state for Ph^+ filaments under these conditions. In contrast to the situation with the Ph^+ filaments, our data suggest that the Ph^- filaments reside in the high-flexibility state even in the absence of myosin. In terms of the proposed model, this suggests that virtually all Ph^- filaments would reside in the A state almost all the time even in the absence of motor activity ($K_{IA} \gg 1$). This prediction should be testable by repeating the experiments of Kozuka et al. (14) using Ph^- filaments.

The high flexibility of Ph^- filaments, also in the absence of myosin, provides evidence that the structural transition between the low- and high-flexibility states is not per se involved in the force-generating structural change in actomyosin. On the other hand, the actin filaments appear to be in the high-flexibility state during actomyosin motor activity for both Ph^+ and Ph^- filaments, under all experimental conditions tested. This is consistent with the idea that transition into the high-flexibility state may be a component of the activation process (cf. (11)), as also recently proposed for the switch from the low- to high-FRET state (14) (Fig. 5 *F*). In addition to actomyosin motor activity, a switch from the low- to the high-flexibility state might be induced by Ca^{2+}-induced movement of the troponin-tropomyosin complex on the surface of actin (11,63). A change in actin structure, leading to increased flexibility may thus be complementary to a removal of steric blocking of myosin binding in the activation process. This idea accords with a markedly reduced persistence length upon Ca^{2+} binding to the troponin-tropomyosin-F-actin complex (3). Moreover, it is interesting to note that the persistence length of troponin-tropomyosin-F-actin filaments in the absence of Ca^{2+} was not further increased by the presence of phalloidin (3). This is again in accordance with the existence of just two different flexibility states (16), where the low-flexibility state is stabilized both by phalloidin and troponin-tropomyosin in the absence of Ca^{2+}.

The small reduction in sliding velocity caused by phalloidin stabilization at high-HMM-incubation concentrations (and thus high-HMM surface densities) is intriguing. At first, we considered the possibility that it may be causally related to a switch of the entire filament from a low-flexibility to a high-flexibility conformation upon motor activity. In this case, maintenance of the actin filaments in the active state may be expected to require energy input, thereby reducing the free energy available for transportation of the filaments. However, if this had been the cause of the lower sliding velocity it would have been expected to occur to an even greater degree at low HMM densities with fewer attached myosin heads, but this was not the case. Tokuraku and Uyeda (52) proposed that the effect of phalloidin stabilization on sliding velocity may be related to the presumed higher flexural rigidity of Ph^+ filaments. However, the results presented here are at variance with this idea. Thus, at low ionic strengths, where the effect of phalloidin stabilization on velocity was most prominent, we observed similar flexibility of motor-propelled Ph^+ and Ph^- filaments. A more likely explanation, in view of the effects of ionic strength and HMM density, is increased drag forces on the Ph^+ filaments due to enhanced electrostatic interactions between the filaments and the HMM-coated surface. Such effects may be brought about if phalloidin binding changes the electrostatic surface potential of the actin filaments, e.g., by subtle changes in actin filament structure.

The different effects of myosin motor activity on the actin filament persistence length in Ph^+ and Ph^- filaments suggests that the actin filament dynamics upon myosin binding and motor activity is different in the presence of phalloidin stabilization than in its absence. This insight, which is contrary to generally held views (14,15) (however, see (52,64)), is of fundamental importance, since studies of actomyosin function routinely rely on the use of phalloidin-stabilized filaments. Results of such studies profoundly affect our view of eukaryotic cell motility due to the ubiquitous presence and importance of actomyosin in this connection.

Implication of results for nanotechnological applications of actomyosin

The results also have implications for nanotechnological applications. Thus, the lower persistence length for Ph^+ filaments during motor-induced sliding compared to per-

sistence length in solution suggests increased potential for miniaturization in lab-on-a-chip devices (see also (37)). In such applications, it may be of interest to transport phalloidin-stabilized filament, including those labeled with biotin-phalloidin (51,65,66), in loops of very small radii (e.g., (53,66)). It is also important to point out in this connection that the persistence length of actin filaments is at least one order of magnitude lower than for kinesin-propelled microtubules (28–30,37), with increased potential for miniaturization of transportation systems.

CONCLUDING REMARKS

In conclusion, we have, for the first time to our knowledge, demonstrated substantial changes in bending flexibility of actin filaments during active sliding on a heavy-meromyosin-coated surface. The results were obtained using a simple in vitro motility assay procedure. Our findings are consistent with important structural changes in actin during activation of actomyosin motor activity, but not during the actual force-generating and actin-propelling step. The finding that there are significant differences between the results with phalloidin-stabilized and phalloidin-free actin filaments challenges the view that these behave in a similar way during their force-generating interaction with myosin molecules. Finally, the results presented in this study have implications for the degree of miniaturization that is possible with lab-on-a-chip applications where molecular motors are used for transportation of actin-attached cargoes.

SUPPLEMENTARY MATERIAL

To view all of the supplemental files associated with this article, visit www.biophysj.org.

Valuable discussions with Dr. Martina Balaz and Professors Sven Tågerud and Roger Karlsson are acknowledged.

This work was supported by grants from The Swedish Research Council (project No. 621-2007-6137), The Carl Trygger Foundation, The Knowledge Foundation (KK-stiftelsen), The Crafoord Foundation, and The Faculty of Natural Sciences and Engineering, University of Kalmar. The authors do not have any conflict of interest.

REFERENCES

1. Huxley, A. F. 1957. Muscle structure and theories of contraction. *Prog. Biophys. Biophys. Chem.* 7:255–318.
2. Geeves, M. A., and K. C. Holmes. 2005. The molecular mechanism of muscle contraction. *Adv. Protein Chem.* 71:161–193.
3. Isambert, H., P. Venier, A. C. Maggs, A. Fattoum, R. Kassab, D. Pantaloni, and M. F. Carlier. 1995. Flexibility of actin filaments derived from thermal fluctuations. Effect of bound nucleotide, phalloidin, and muscle regulatory proteins. *J. Biol. Chem.* 270:11437–11444.
4. Orlova, A., E. Prochniewicz, and E. H. Egelman. 1995. Structural dynamics of F-actin: II. Cooperativity in structural transitions. *J. Mol. Biol.* 245:598–607.
5. Schutt, C. E., J. C. Myslik, M. D. Rozycki, N. C. Goonesekere, and U. Lindberg. 1993. The structure of crystalline profilin-β-actin. *Nature.* 365:810–816.
6. Greenberg, M. J., C. L. Wang, W. Lehman, and J. R. Moore. 2008. Modulation of actin mechanics by caldesmon and tropomyosin. *Cell Motil. Cytoskeleton.* 65:156–164.
7. Yanagida, T., and F. Oosawa. 1978. Polarized fluorescence from epsilon-ADP incorporated into F-actin in a myosin-free single fiber: conformation of F-actin and changes induced in it by heavy meromyosin. *J. Mol. Biol.* 126:507–524.
8. Prochniewicz, E., and D. D. Thomas. 2001. Site-specific mutations in the myosin binding sites of actin affect structural transitions that control myosin binding. *Biochemistry.* 40:13933–13940.
9. Shimo, R., and K. Mihashi. 2001. Fluctuation of local points of F-actin sliding on the surface-fixed H-meromyosin molecules in the presence of ATP. *Biophys. Chem.* 93:23–35.
10. Borovikov, Y. S., I. V. Dedova, C. G. dos Remedios, N. N. Vikhoreva, P. G. Vikhorev, S. V. Avrova, T. L. Hazlett, and B. W. Van Der Meer. 2004. Fluorescence depolarization of actin filaments in reconstructed myofibers: the effect of S1 or pPDM-S1 on movements of distinct areas of actin. *Biophys. J.* 86:3020–3029.
11. Egelman, E. H., and A. Orlova. 1995. New insights into actin filament dynamics. *Curr. Opin. Struct. Biol.* 5:172–180.
12. Takebayashi, T., Y. Morita, and F. Oosawa. 1977. Electronmicroscopic investigation of the flexibility of F-actin. *Biochim. Biophys. Acta.* 492:357–363.
13. Orlova, A., and E. H. Egelman. 1997. Cooperative rigor binding of myosin to actin is a function of F-actin structure. *J. Mol. Biol.* 265:469–474.
14. Kozuka, J., H. Yokota, Y. Arai, Y. Ishii, and T. Yanagida. 2006. Dynamic polymorphism of single actin molecules in the actin filament. *Nat. Chem. Biol.* 2:83–86.
15. Prochniewicz, E., T. F. Walseth, and D. D. Thomas. 2004. Structural dynamics of actin during active interaction with myosin: different effects of weakly and strongly bound myosin heads. *Biochemistry.* 43:10642–10652.
16. Orlova, A., and E. H. Egelman. 1993. A conformational change in the actin subunit can change the flexibility of the actin filament. *J. Mol. Biol.* 232:334–341.
17. Yanagida, T., M. Nakase, K. Nishiyama, and F. Oosawa. 1984. Direct observation of motion of single F-actin filaments in the presence of myosin. *Nature.* 307:58–60.
18. Prochniewicz, E., E. Katayama, T. Yanagida, and D. D. Thomas. 1993. Cooperativity in F-actin: chemical modifications of actin monomers affect the functional interactions of myosin with unmodified monomers in the same actin filament. *Biophys. J.* 65:113–123.
19. Bugyi, B., G. Papp, G. Hild, D. Lorinczy, E. M. Nevalainen, P. Lappalainen, B. Somogyi, and M. Nyitrai. 2006. Formins regulate actin filament flexibility through long range allosteric interactions. *J. Biol. Chem.* 281:10727–10736.
20. Kitamura, K., M. Tokunaga, A. H. Iwane, and T. Yanagida. 1999. A single myosin head moves along an actin filament with regular steps of 5.3 nanometres. *Nature.* 397:129–134 [see comments].
21. Yanagida, T., and Y. Ishii. 2003. Stochastic processes in nano-biomachines revealed by single molecule detection. *Biosystems.* 71: 233–244.
22. Schutt, C. E., and U. Lindberg. 1992. Actin as the generator of tension during muscle contraction. *Proc. Natl. Acad. Sci. USA.* 89:319–323.
23. Cooke, R. 1997. Actomyosin interaction in striated muscle. *Physiol. Rev.* 77:671–697.
24. Spudich, J. A. 2001. The myosin swinging cross-bridge model. *Nat. Rev. Mol. Cell Biol.* 2:387–392.
25. Burlacu, S., and J. Borejdo. 1992. Motion of actin filaments in the presence of myosin heads and ATP. *Biophys. J.* 63:1471–1482.
26. Le Goff, L., F. Amblard, and E. M. Furst. 2002. Motor-driven dynamics in actin-myosin networks. *Phys. Rev. Lett.* 88:018101.

27. Duke, T., T. E. Holy, and S. Leibler. 1995. Gliding assays for motor proteins: a theoretical analysis. *Phys. Rev. Lett.* 74:330–333.

28. Nitta, T., and H. Hess. 2005. Dispersion in active transport by kinesin-powered molecular shuttles. *Nano Lett.* 5:1337–1342.

29. van den Heuvel, M. G., M. P. de Graaff, and C. Dekker. 2008. Microtubule curvatures under perpendicular electric forces reveal a low persistence length. *Proc. Natl. Acad. Sci. USA.* 105:7941–7946.

30. van den Heuvel, M. G., S. Bolhuis, and C. Dekker. 2007. Persistence length measurements from stochastic single-microtubule trajectories. *Nano Lett.* 7:3138–3144.

31. Pampaloni, F., G. Lattanzi, A. Jonas, T. Surrey, E. Frey, and E. L. Florin. 2006. Thermal fluctuations of grafted microtubules provide evidence of a length-dependent persistence length. *Proc. Natl. Acad. Sci. USA.* 103:10248–10253.

32. Gittes, F., B. Mickey, J. Nettleton, and J. Howard. 1993. Flexural rigidity of microtubules and actin filaments measured from thermal fluctuations in shape. *J. Cell Biol.* 120:923–934.

33. Chu, J. W., and G. A. Voth. 2005. Allostery of actin filaments: molecular dynamics simulations and coarse-grained analysis. *Proc. Natl. Acad. Sci. USA.* 102:13111–13116.

34. Chu, J. W., and G. A. Voth. 2006. Coarse-grained modeling of the actin filament derived from atomistic-scale simulations. *Biophys. J.* 90:1572–1582.

35. Nishizaka, T., T. Yagi, Y. Tanaka, and S. Ishiwata. 1993. Right-handed rotation of an actin filament in an in vitro motile system. *Nature.* 361:269–271.

36. Kraikivski, P., R. Lipowsky, and J. Kierfeld. 2006. Enhanced ordering of interacting filaments by molecular motors. *Phys. Rev. Lett.* 96:258103.

37. Nitta, T., A. Tanahashi, Y. Obara, M. Hirano, M. Razumova, M. Regnier, and H. Hess. 2008. Comparing guiding track requirements for myosin- and kinesin-powered molecular shuttles. *Nano Lett.* 8:2305–2309.

38. Ott, A., M. Magnasco, A. Simon, and A. Libchaber. 1993. Measurement of the persistence length of polymerized actin using fluorescence microscopy. *Phys. Rev. E Stat. Phys. Plasmas Fluids Relat. Interdiscip. Topics.* 48:R1642–R1645.

39. Yasuda, R., H. Miyata, and K. Kinosita. 1996. Direct measurement of the torsional rigidity of single actin filaments. *J. Mol. Biol.* 263:227–236.

40. Howard, J. 2001 Mechanics of Motor Proteins and the Cytoskeleton. Sinauer Associates, Sunderland, MA.

41. Rivetti, C., M. Guthold, and C. Bustamante. 1996. Scanning force microscopy of DNA deposited onto mica: equilibration versus kinetic trapping studied by statistical polymer chain analysis. *J. Mol. Biol.* 264:919–932.

42. Harada, Y., K. Sakurada, T. Aoki, D. D. Thomas, and T. Yanagida. 1990. Mechanochemical coupling in actomyosin energy transduction studied by in vitro movement assay. *J. Mol. Biol.* 216:49–68.

43. Albet-Torres, N., J. O'Mahony, C. Charlton, M. Balaz, P. Lisboa, T. Aastrup, A. Månsson, and I. A. Nicholls. 2007. Mode of heavy meromyosin adsorption and motor function correlated with surface hydrophobicity and charge. *Langmuir.* 23:11147–11156.

44. Kron, S. J., Y. Y. Toyoshima, T. Q. Uyeda, and J. A. Spudich. 1991. Assays for actin sliding movement over myosin-coated surfaces. *Methods Enzymol.* 196:399–416.

45. Pardee, J. D., and J. A. Spudich. 1982. Purification of muscle actin. *Methods Cell Biol.* 24:271–289.

46. Dedova, I. V., S. V. Avrova, N. N. Vikhoreva, R. G. Vikhorev, T. L. Hazlett, W. Van der Meer, C. G. Dos Remedios, and S. Borovikov Iu. 2004. Conformational changes of actin induced by strong or weak myosin subfragment-1 binding. *Tsitologiia.* 46:719–734.

47. Sundberg, M., J. P. Rosengren, R. Bunk, J. Lindahl, I. A. Nicholls, S. Tagerud, P. Omling, L. Montelius, and A. Månsson. 2003. Silanized surfaces for in vitro studies of actomyosin function and nanotechnology applications. *Anal. Biochem.* 323:127–138.

48. Klinth, J., A. Arner, and A. Mansson. 2003. Cardiotonic bipyridine amrinone slows myosin-induced actin filament sliding at saturating. *J. Muscle Res. Cell Motil.* 24:15–32 [MgATP].

49. Månsson, A., and S. Tagerud. 2003. Multivariate statistics in analysis of data from the in vitro motility assay. *Anal. Biochem.* 314:281–293.

50. Bourdieu, L., T. Duke, M. B. Elowitz, D. A. Winkelmann, S. Leibler, and A. Libchaber. 1995. Spiral defects in motility assays: a measure of motor protein force. *Phys. Rev. Lett.* 75:176–179.

51. Balaz, M., and A. Mansson. 2005. Detection of small differences in actomyosin function using actin labeled with different phalloidin conjugates. *Anal. Biochem.* 338:224–236.

52. Tokuraku, K., and T. Q. P. Uyeda. 2001. Phalloidin affects the myosin-dependent sliding velocities of actin filaments in a bound-divalent cation dependent manner. *J. Muscle Res. Cell Motil.* 22:371–378.

53. Sundberg, M., R. Bunk, N. Albet-Torres, A. Kvennefors, F. Persson, L. Montelius, I. A. Nicholls, S. Ghatnekar-Nilsson, P. Omling, S. Tagerud, and A. Mansson. 2006. Actin filament guidance on a chip: toward high-throughput assays and lab-on-a-chip applications. *Langmuir.* 22:7286–7295.

54. Sundberg, M., M. Balaz, R. Bunk, J. P. Rosengren-Holmberg, L. Montelius, I. A. Nicholls, P. Omling, S. Tagerud, and A. Månsson. 2006. Selective spatial localization of actomyosin motor function by chemical surface patterning. *Langmuir.* 22:7302–7312.

55. Grazi, E., E. Magri, and L. Rizzieri. 1989. The influence of sub-stoichiometric concentrations of myosin subfragment 1 on the state of aggregation of actin under depolymerizing conditions. *Eur. J. Biochem.* 182:277–282.

56. Burlacu, S., P. A. Janmey, and J. Borejdo. 1992. Distribution of actin filament lengths measured by fluorescence microscopy. *Am. J. Physiol.* 262:C569–C577.

57. Pavlov, D., A. Muhlrad, J. Cooper, M. Wear, and E. Reisler. 2007. Actin filament severing by cofilin. *J. Mol. Biol.* 365:1350–1358.

58. Liu, X., and G. H. Pollack. 2002. Mechanics of F-actin characterized with microfabricated cantilevers. *Biophys. J.* 83:2705–2715.

59. Arii, Y., and K. Hatori. 2008. Relationship between the flexibility and the motility of actin filaments: effects of pH. *Biochem. Biophys. Res. Commun.* 371:772–776.

60. Steinmetz, M. O., K. N. Goldie, and U. Aebi. 1997. A correlative analysis of actin filament assembly, structure, and dynamics. *J. Cell Biol.* 138:559–574.

61. Lorenz, M., D. Popp, and K. C. Holmes. 1993. Refinement of the F-actin model against X-ray fiber diffraction data by the use of a directed mutation algorithm. *J. Mol. Biol.* 234:826–836.

62. Kim, E., E. Bobkova, G. Hegyi, A. Muhlrad, and E. Reisler. 2002. Actin cross-linking and inhibition of the actomyosin motor. *Biochemistry.* 41:86–93.

63. Homsher, E., M. Nili, I. Y. Chen, and L. S. Tobacman. 2003. Regulatory proteins alter nucleotide binding to acto-myosin of sliding filaments in motility assays. *Biophys. J.* 85:1046–1052.

64. Adami, R., O. Cintio, G. Trombetta, D. Choquet, and E. Grazi. 2002. Effects of chemical modification, tropomyosin, and myosin subfragment 1 on the yield strength and critical concentration of F-actin. *Biochemistry.* 41:5907–5912.

65. Månsson, A., M. Sundberg, M. Balaz, R. Bunk, I. A. Nicholls, P. Omling, S. Tågerud, and L. Montelius. 2004. In vitro sliding of actin filaments labelled with single quantum dots. *Biochem. Biophys. Res. Commun.* 314:529–534.

66. Månsson, A., M. Sundberg, R. Bunk, M. Balaz, I. A. Nicholls, P. Omling, J. O. Tegenfeldt, S. Tågerud, and L. Montelius. 2005. Actin-based molecular motors for cargo transportation in nanotechnology: potentials and challenges. *IEEE Trans. Adv. Pack.* 28:547–555.